


RESEARCH ARTICLE

Open Access



# RH simulation model for canvas paintings protected by an aluminium backplate and an additional hygroscopic layer

Santi Ferrer<sup>1</sup>, Gema Campo-Francés<sup>2</sup>, Josep Grau-Bové<sup>3</sup>, Iris Bautista-Morenilla<sup>2\*</sup>  and Anna Nualart-Torroja<sup>2</sup>

## Abstract

To protect a canvas easel painting, a common conservation strategy is to add a back plate at the stretcher, creating a closed air void. This plate protects not only from dust but mainly from temperature and relative humidity (*RH*) variations in the room and moisture changes in the wall on which it is hanging. The addition of hygroscopic layers can reduce the amplitude and change phase of humidity oscillations. This paper proposes a new mathematical model that can be used to predict moisture levels within the canvas when this conservation strategy is applied. The model is compared against the temperature and *RH* detailed experimental data, captured and shown in the latest paper by Padfield et al. *Back protection of canvas painting*. Our paper presents values of *T*, *RH* and mixing ratio (*MR*) obtained at the different layers of an easel painting, protected and unprotected, with cotton and without it, submitted to different room and wall temperature and *RH* cycles. The experimental results show a phase displacement between the canvas temperatures and the corresponding *RH* values in the canvas air boundary layer. In some cases this phase shift, which is an unexpected behaviour, allows *RH* and temperatures to achieve their maximum value at the same time. The purpose of the model is to simulate the *RH* response at the different air boundary layers inside the air void, such as the canvas, the aluminium back plate, and the hygroscopic cotton protection, produced by cyclic variations of temperature in the room or the wall. The model is built simulating four interrelated processes: the canvas permeation flow, the air infiltration rate between room and void, the equilibrium moisture content (*EMC*) and the vapour sorption rate for the canvas and the cotton. A key innovation of the model is the dependence between *EMC*, sorption rate, and *RH* condition, which captures the counter-intuitive behaviours observed in the data. The model results agree with the experimental results. The developed tool allows the interpretation of the processes involved and to extend the simulations to other cases, materials, and conditions.

**Keywords:** Painting conservation, Canvas protections simulation, Canvas permeation, Linen sorption, Cotton sorption, *EMC*

## Introduction

Most of the materials that are part of canvas easel paintings, such as canvas, size, ground, and painting layers, when subjected to changes in relative humidity over time, suffer size fluctuations, contractions, expansions, and

ripples which affect their correct conservation. Contractions of these materials, which are fixed to the stretcher through the canvas, increase internal stresses and can, if their elastic limit is surpassed, result in permanent deformation or fracture. Relative humidity fluctuations can occur in poorly insulated buildings where the climate is dominated by outside conditions or in spaces without proper temperature and humidity control. Inappropriate relative humidity conditions can also occur due to temperature gradients in rooms with controlled

\*Correspondence: [ibautista@ub.edu](mailto:ibautista@ub.edu)

<sup>2</sup> Arts and Conservation Department, Fine Arts Faculty, University of Barcelona, C/Pau Gargallo 4, 08028 Barcelona, Spain  
Full list of author information is available at the end of the article

temperatures but with paintings hanging on non-insulated exterior walls.

These problems and the damage that they cause on the paintings have been studied by researchers such as Mecklenburg [1, 2], who has modelled the mechanical response of materials to changes in humidity and temperature, Von Reden [3], who has analysed experimentally the interactions of canvas and relative humidity, or Berger [4, 5], who in his studies analyses the deterioration of surfaces exposed to environmental changes and the behaviour of the canvas as a support for paintings, and also Michalski [6], who has studied from different points of view the response of paintings to temperature and relative humidity. This body of research has resulted in guidelines as Michalski [7], ASHRAE [8], and EN 15757 [9].

Another approach to studying the problem of climatic conditions that affect cultural heritage has been the mathematical model simulations, for example with CFDs such as Ferrer et al. [10], which analyse the conditions that occur in the space between the back of a painted wood panel and a cold wall. Other studies that use CFDs are discussed in the article on Grau-Bové [11]. Other mathematical models, such as the ones developed by Di Pietro–Ligterink [12, 13], have been experimentally tested to confirm their validity. These works have demonstrated the ability of mathematical modelling to predict micro-environmental conditions and support the development of preventive conservation solutions.

When indoor climate conditions cannot be controlled, other procedures must be applied to limit damage to paintings by implementing passive micro-environmental control. One of these procedures is the incorporation of a back protection [14, 15]. In recent years, aluminium back plates have been attached to the stretcher, building an air void that insulates the canvas from the wall, and obtaining a temperature in the air void which is close to the controlled room temperature thanks to the aluminium thermal conduction. This protection can be improved by introducing a cotton layer inside the void, in order to stabilize the void air relative humidity ( $RH$ ) by the cotton adsorption/desorption of water vapour.

In his last paper, Padfield et al. [16] show the experimental relative humidity ( $RH$ ) and mixing ratio ( $MR$ ) values obtained from different room cycle temperatures and wall cycle temperatures, in the different layers of an open woven linen canvas with a factory applied ground and a coat of white acrylic paint fixed at a wood stretcher, unprotected, or protected by an aluminium back plate (in one case also with glass protection over the canvas) and with or without a cotton hygroscopic layer in the void.

In the cases of room temperature variations (with cotton and without it) and in the case of wall temperature

variations and existence of a cotton layer, a delay appears between the  $RH$  obtained values in the canvas air boundary layer and the expected  $RH$  values according to the canvas temperatures. In some cases, the delay attained is so large that the  $T$  and  $RH$  of the canvas increase and decrease simultaneously, even when externally they fluctuate in an opposite way, as usually expected. This surprising fact is acknowledged in the Padfield paper [16] figs. 11, 14 and 15], and similar processes have been observed experimentally in comparable systems [12]. However, to date this process has not been explained fully with a complete mathematical-physical model.

To avoid condensation or damage inside the void it is important to accurately predict the  $RH$  values attained there, according to the foreseen temperatures and  $RH$  values at the wall and the room and other factors such as the cotton and linen mass, its location in the void and the vapour exchange between the room and the void.

Our research is focused on developing a mathematical model to explain and simulate accurately the  $RH$  phase displacements from temperature, in order to understand the interactions between the different processes involved.

To build the mathematical model, the equations corresponding at the four partial processes involved in the  $MR$  and  $RH$  changes at the void between canvas and aluminium, when the room, void, canvas, aluminium and cotton temperatures changes along the time, shall be developed. These processes are: the canvas vapour permeation, the air infiltration between inside the void and the room, the cotton vapour sorption, and the canvas vapour sorption inside the void. A relevant aspect to consider is whether the sorption of water into the wood stretcher is high enough to be included in the model. Previous research has shown that the effect of the stretcher in buffering is negligibly small, according Ligterink and Di Pietro [13 Sect. 5] for similar cases, despite its considerable mass in comparison to other components of the painting. For this reason, the model presented in this paper does not include water sorption in the stretcher, even though we recognise it is a matter of current scientific debate and there may be scenarios where its role in buffering is indeed significant.

All these four processes depend on the  $RH$  values at the room, the void and the air boundary layers close to the canvas, aluminium and cotton. The interactions between them are very complex and solving the differential equations involved, requires a numerical procedure following a finite element method (FEM) approach. In other words dividing the temperature cycles in time steps and calculating, for each time step, the vapour flow and the change of mixing ratio ( $\Delta MR$ ) for each process in parallel, to get the total  $\Delta MR$  and the  $MR$  in the void at the end of each

time step. The time steps shall be short enough to allow a stable calculation and the required accuracy.

We have compared our results with the experimental data by Padfield and al. [16 Figs. 7, 11, 14 and 15], using the same start conditions and temperatures cycles observing a close agreement between.

This model provides a tool for to examine the hygro-thermal behaviour of this complex system, allowing researchers to investigate the consequences of different canvas protection strategies under any thermo-hygro-metric conditions.

**Studied cases**

We have selected four representative cases to be modelled, shown in Fig. 1. These cases cover the full range of preservation options included in the model: aluminium back plate, internal cotton for buffering and glass in front of the painting. The RH oscillated in different cycle frequencies (4 and 24 h). The experimental data used to

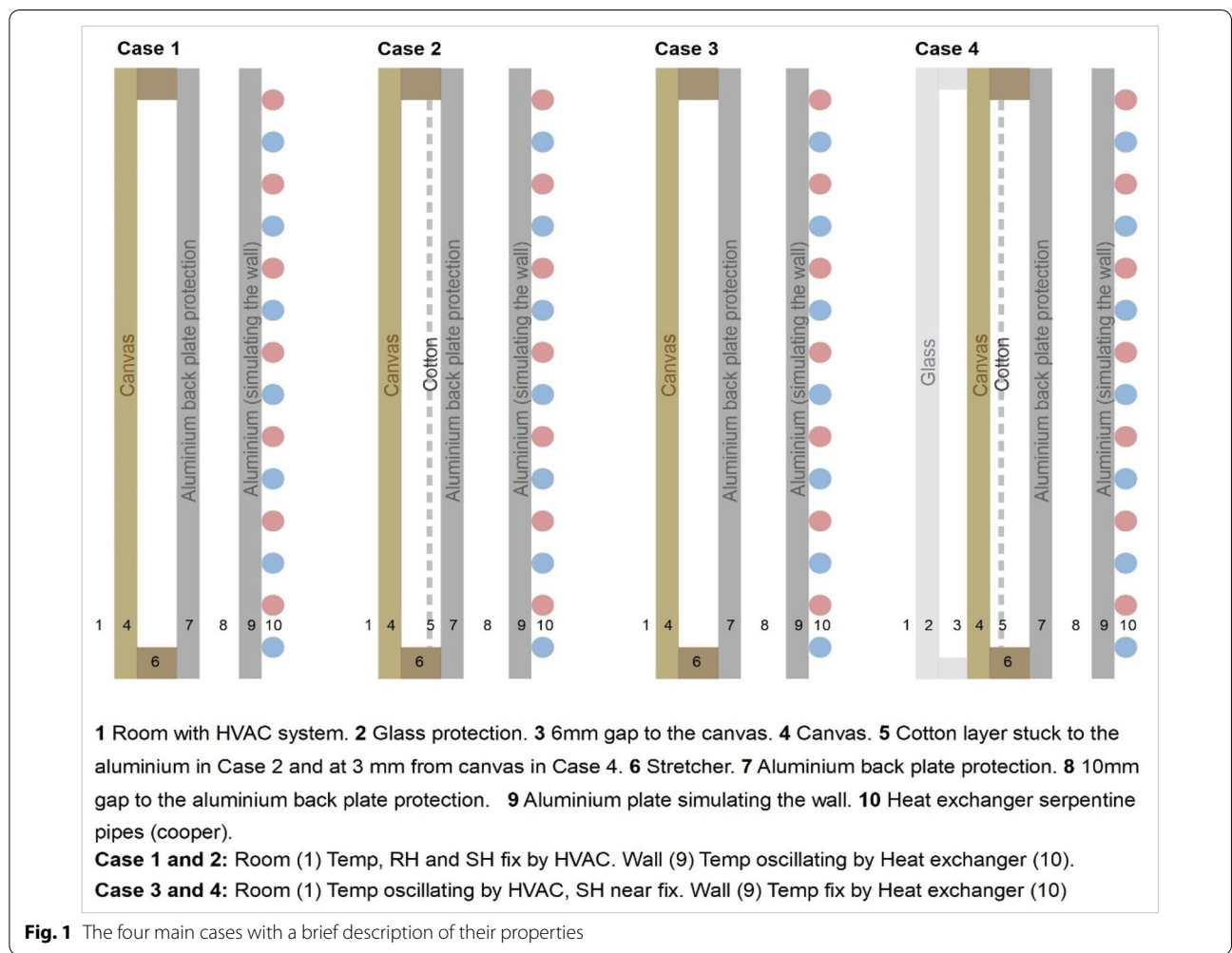
validate the model is provided in the paper by Padfield et al. [Figs. 7, 11, 14 and 15 of reference 16].

**Case 1 according [16 Fig. 7]**

Linen canvas with ground and a white acrylic layer, nailed to a wood stretcher and an aluminium back plate protection, hung in a room wall. The cycle temperatures have a 4-h cycle. The  $T_{room}$  is 27 °C with  $\Delta T = \pm 0.2$  K. These conditions are achieved by the room HVAC system and the  $MR_{room}$  is kept fixed at 11.11 g/kg.

The  $T_{alum}$  is 24 °C with  $\Delta T = \pm 3$  K and the  $T_{canv}$  is 25 °C and with  $\Delta T = \pm 1$  K along the cycles. These conditions are achieved by a serpentine plate coil heat exchanger (copper pipes and aluminium plate) with an aluminium plate, simulating the wall and located 10 mm behind the aluminium back plate protection.

The  $MR$  initial condition in the void between the canvas and the aluminium back plate protection is 11.88 g/kg which corresponds to 25 °C and 60% RH at the canvas,



and it will change along the temperature cycles by the partial processes involved in this case which are canvas permeation, air infiltration and canvas vapour sorption.

**Case 2 according [16 Fig. 11]**

The same materials and geometry as Case 1 but with a cotton layer attached to the aluminium inside the void. The cycle temperatures have a 4-h cycle. The  $T_{room}$  is 26.5 °C, the  $RH_{room}$  is 52% and the  $MR_{room}$  11.435 g/kg all them fix and achieved by the room HVAC system.

The  $T_{alum}$  is 24.75 °C with  $\Delta T = \pm 5.9$  K along the cycle and it is achieved by the serpentine heat exchanger. The  $T_{canv}$  is 24.8 °C with  $\Delta T = \pm 3.3$  K. Cotton values do not appear in [16 Fig. 11] but as should be close to the aluminium temperature, due to its position, values of 24.78 °C  $\pm 5.5$  K have been used in our model for cotton.

The  $MR$  initial conditions in the void between the canvas and the aluminium back plate protection are 11.53 g/kg corresponding to the 24.8 °C and 58.2%  $RH$  conditions at canvas start. They will change along the temperature cycles by the partial processes involved.

**Case 3 according [16 Fig. 14]**

The same materials and geometry as Case 1 but the room temperatures have a 24-h cycle. The  $T_{room}$  is 25 °C with  $\Delta T = \pm 7$  K achieved by a HVAC system and the wall temperature simulated by the serpentine coil heat exchanger and the aluminium plate is nearly constant. The initial  $MR_{room}$  starts at 11.58 g/kg corresponding to a  $T_{room} = 25$  °C and  $RH = 58.5\%$ , descending lineally down to 10.78 g/kg 48 h later. The  $T_{alum}$  is 24.4 °C with  $\Delta T = \pm 2$  K and the start  $T_{canv}$  is 24.6 °C with  $\Delta T = \pm 5.2$  K along the cycle. The  $MR$  start at canvas is 11.59 g/kg which corresponds to 24.6 °C and 60%  $RH$ .

**Case 4 according [16 Fig. 15]**

The same materials and geometry as Case 2 but with the cotton layer at 3 mm from the canvas and inside the void. The room temperatures have a 24-h cycle. The  $T_{room}$  is 25 °C with  $\Delta T = \pm 6.5$  K achieved by a HVAC system and the wall temperature simulated by the serpentine coil heat exchanger. The  $T_{canv}$  is 24.9 °C with  $\Delta T = \pm 3.85$  K and the  $T_{alum}$  is 24.8 °C with  $\Delta T = \pm 1.2$  K.

At [16 Fig. 15] in the  $MR$  graphic the  $MR$  values increases a step in the second cycle and an  $MR$  control error appears at the end of the second cycle. It is supposed to be an experimental problem. To deal with it in our simulation the initial  $MR_{room}$  starts at 11.83 g/kg corresponding to a  $T_{room} = 25$  °C and  $RH = 59\%$  and increases lineally up to 12.23 g/kg, at the end of the second cycle 48 h later. For the canvas void (between the canvas and the cotton) the start  $RH$  is 65.5% at canvas which corresponds to a start  $MR_{void}$  of 13.06 g/kg.

Cotton values do not appear in [16 Fig. 15] graphic. As the cotton temperature should be close to the canvas one, due to its position, we have used for cotton cycle temperatures  $T_{cott} = 24.9$  °C and  $\Delta T = \pm 3.9$  K.

**Model development**

The model considers four partial processes of mass exchange (Fig. 2), driven by the differences in moisture concentration: (i) permeation and (ii) infiltration from the room to the void through the canvas, (iii) sorption between the void and the canvas and (iv) sorption between the cotton layer and the void. We assume that other mass transfer processes that may occur in this system are negligible in comparison to these four. In particular, the model assumes that the transference of moisture between the void and the wood of the stretcher is negligible small. This may seem surprising given the high relative mass of the wood compared with other materials, but previous research indicates that this assumption is reasonable. Thybring [17] estimates the water vapour diffusivity in wood ranging from  $10^{-13}$  to  $10^{-11}$  m<sup>2</sup>/s. For textiles, as cotton canvas, the values are from  $10^{-9}$  to  $10^{-8}$  m<sup>2</sup>/s from Henry [18].

Another key assumption is that any potential gradients of water concentration within the canvas and cotton do not affect the rate of processes 1, 3 and 4 i.e., that these materials can be modelled with a lumped parameter approach.

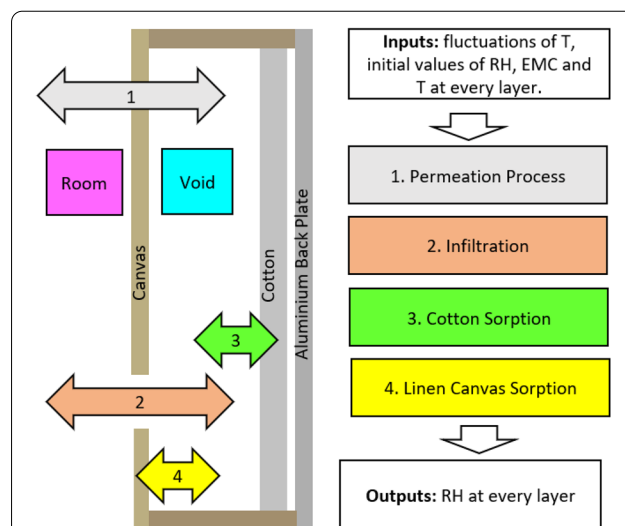


**Fig. 2** Schematic representation of the four partial processes and the main inputs and outputs. The colours correspond with Fig. 5, and the number of the processes to the description in “Humidity change at the void from the vapour permeation through the canvas (Partial process 1)” to “Humidity change at the void from the vapour sorption in the linen canvas (Partial process 4)” sections

### Calculation procedure by time steps

The calculation procedure takes place time step by time step. At the time step zero the temperatures and *RH* do not change, and we calculate the mixing ratios, *MR room* and *MR void*, with the initial temperatures and the *RH* values at the room and the void. We use:

$$MR = 0.622 \cdot \left(\frac{RH}{100}\right) \cdot P_{sat} / \left(P_{atm} - \left(\frac{RH}{100}\right) \cdot P_{sat}\right) \tag{1}$$

We have chosen to use an equation for *psat* which is accurate at a wide range of temperatures [19]:

$$\begin{aligned} \text{For } T \geq 0 \quad psat &= e^{\frac{17.269 \cdot T}{237.3 + T}} \\ \text{For } T < 0 \quad psat &= e^{\frac{21.875 \cdot T}{265.5 + T}} \end{aligned} \tag{1a}$$

At the start of time step one, the temperature changes in all points (Room, Void, Canvas, Aluminium and Cotton) and thus the *RH* values change as well. From the initial *MR Void* value and the new temperature values we calculate the new *RH* values for the Canvas, Aluminium and Cotton layers at the start of the time step one:

$$RH_{layer} = 100 \cdot MR_{void} \cdot P_{atm} / (P_{sat\ layer} \cdot (0.622 + MR_{void})) \tag{1b}$$

With *layer* as *canv*, *alum* and *cott*, and using (1a) for *psat*. We obtain the new *MR room* with Eqs. (1 and 1a) from the news *T room* and *RH room*.

From these values we can find, in the current time step, the increase of mixing ratio ( $\Delta MR$ ) in the void from each partial process by following the calculations for each of them, as described in from “Humidity change at the void from the vapour permeation through the canvas (Partial process 1)” to “Humidity change at the void from the vapour sorption in the linen canvas (Partial process 4)” sections. At the end of each time step we calculate the total increase of mixing ratio in the void ( $\Delta MR_{void}$ ), and thus obtain the new *MR void*. Once this is known, the time step ends, and we can repeat the calculation procedure for the next time step. This iterating procedure, time step by time step, allows us to calculate the evolution of the system for as long as necessary.

### Cycle temperatures calculation for each time step

The time steps used in modelling need to be far smaller than the frequency of measurements of the experimental data. As a result, it is efficient to replace the temperature input data (*T canv*, *T cott*, *T room* and *T alum*) by values calculated with a harmonic oscillation, which fits perfectly with the data used in this case. For any of the locations of interest:

$$T_i = T_{start} + \Delta T \cdot \cos(\beta + t_i \cdot \omega)$$

where  $\beta$  (rad) and  $\omega$  are fitted to the data of each studied case (Additional file 1). This strategy is possible thanks to the oscillating shape of the input data. To use the model with non-oscillating data, it would be necessary to interpolate the values of *T* in order to obtain a time-series with time-steps that match the calculation. If the thermal resistance of each layer is known, it is also possible to predict the temperature in every layer given the external temperature. However, this is outside the scope of this paper.

### Humidity change at the void from the vapour permeation through the canvas (Partial process 1)

The water vapour flows by permeation through the canvas between the void and the room (first partial process). It depends on the canvas permeance and the *RH* in both canvas sides. To calculate the *MR void perm<sub>i</sub>* we use:

$$\frac{dM_{vap\ void\ perm}}{dt} = P \cdot A \cdot (P_{vap\ room} - P_{vap\ canv}) \tag{2}$$

where *Mvap void perm* is the mass vapour permeation flow (kg), *P* is the Permeance (kg/(m<sup>2</sup> s Pa), *A* is the area (m<sup>2</sup>), *t* is the time (s), and *Pvap* is the vapour pressure (Pa).

As in this equation the variable *RH canv* depends on the canvas and room temperatures, which change along the cycles, it shall be solved by a numerical FEM method, integrating in a discrete way by time steps along the cycles, as explained at point 1 and 3.1, with *Tcanv<sub>i</sub>* and *Troom<sub>i</sub>*, both fixed at each time step. From Eq. (2) we get Eq. (3) and it is:

$$\begin{aligned} \Delta M_{vap\ void\ perm_i} &= P \cdot A \cdot \Delta t \cdot [P_{sat\ room_i} \\ &\quad \cdot (RH_{room_i}/100) - P_{sat\ canv_i} \\ &\quad \cdot (RH_{canv_i}/100)] \end{aligned}$$

where  $\Delta t$  is the time step.

The vapour mass inside the void by permeation at the end of the time step *i* is:

$$M_{vap\ void\ perm_i} = M_{vap\ void_{i-1}} + \Delta M_{vap\ void\ perm_i} \tag{3a}$$

and

$$MR_{void\ perm_i} = M_{vap\ void\ perm_i} / (\rho_{air\ void_i} \cdot Vol_{void}) \tag{3b}$$

With: *MR void perm<sub>i</sub>* in kg vapour/kg/air;  $\rho_{air\ void_i}$  in kg/m<sup>3</sup>; *Vol void* in m<sup>3</sup>.

The  $\Delta MR \text{ void perm}_i$  obtained by the canvas permeation process along this time step is:

$$\Delta MR \text{ void perm}_i = (MR \text{ void perm}_i - MR \text{ void}_{i-1}) \text{ in (kg vapour/kg air)} \tag{3c}$$

**Humidity change at the void from the air infiltration flow (Partial process 2)**

The vapour flow through the space between canvas and stretcher is the second partial process and it depends on the air infiltration rate (volumes/h in the void) and thus on the air-tightness of the canvas attachment to the stretcher (e.g. tension in the canvas, staples distances between them) and possible holes.

Appendix A.1 shows the development and solution of the differential equation that models the air infiltration rate and we get the Eq. (4), which allows us to calculate the vapour concentration in the void by the air infiltration after time interval  $\Delta t$ :

$$CsB = Ce + (CsA - Ce) \cdot \exp(-\Delta t \cdot nVol/h \cdot \rho \text{ rate}) \tag{4}$$

With:

$CsA$  (vapour concentration in the void at the start of time step  $i$ ) =  $MR \text{ void}_{i-1}$ .

$CsB$  (vapour concentration at the end of time step  $i$ ) =  $MR \text{ void}_i$ .

$Ce$  (vapour concentration in room air) =  $MR \text{ room}_i$ .

$nVol/h$  (air infiltration rate at the void in Volumes/h).

$\rho \text{ rate}$  (density rate) =  $\rho \text{ room}/\rho \text{ void}$ .

By the air infiltration process at the end of time step “i” we get  $MR \text{ void inf}_i = CsB$  and:

$$\Delta MR \text{ void inf}_i = MR \text{ void inf}_i - MR \text{ void}_{i-1} \tag{5}$$

**Humidity change at the void from vapour sorption in the cotton layer (Partial process 3)**

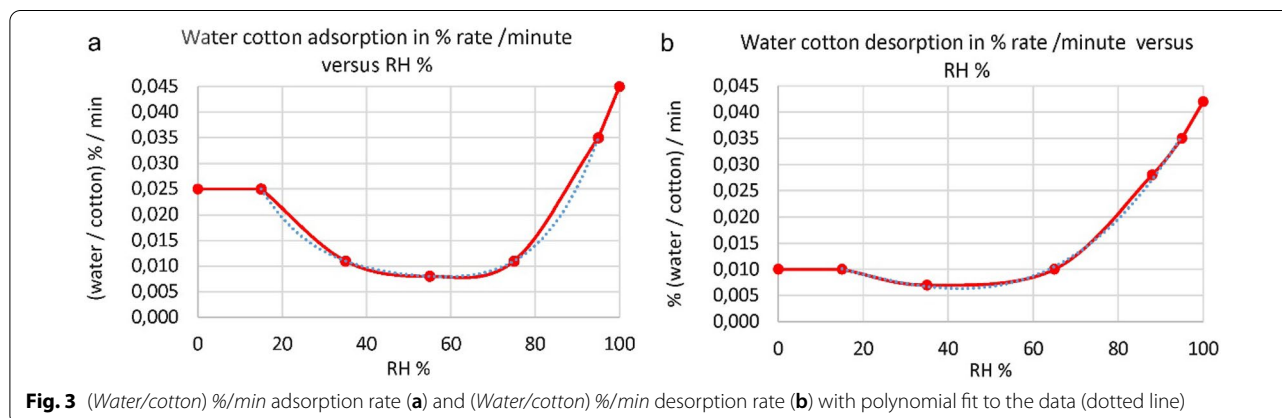
The cotton vapour sorption is the third partial process involved and it depends on two factors:

Sorption factor 1: The *Cotton Sorption rate (%/min)* along the cycle depends on the sorption mode (adsorption or desorption) and on the *RH* values at air boundary layer facing the cotton (*RH cott*). Sorption factor 2: The cotton *EMC* (equilibrium moisture content) limits the amount of water adsorbed in the cotton. It depends on the sorption mode (adsorption or desorption) and on the *RH cott*.

If the *EMC* is attained and the void receives more water vapour, it accumulates temporarily inside the void, increasing the void *MR void* and displacing the *RH cott* cycle phase from the cotton temperature cycle phase. This fact affects the other partial processes as they depend also on the void *RH* values.

To deal with factor 1 we have fitted one equation to the adsorption rate and other equation to the desorption rate, both describe a relationship between *Cotton Sorption rate (%/min)* and *RH*. The values used come from the averaged values at five points in the 4 graphics for Dark/Brown Cotton in Ceylan et al. [20 Fig. 4, lines 3, 6, 9 and 12]. See our Fig. 3a and b.

From these averaged values, in the range of  $15\% < RH < 95\%$ , we have adjusted a 4th order polynomial Eq. (6a) for adsorption and another 3rd order polynomial Eq. (6b) for desorption, using the Solver Excel tool by the GRG (Generalized Reduced Gradient) non-linear method. The large number of significant figures is necessary to obtain a good estimation of the EMC.



For  $RH > 15\%$  :  $WADS(\%rate/min)$   
 $= 0.0000000052 \cdot RH\ cott^4 - 0.0000010417$   
 $\cdot RH\ cott^3 + 0.0000827604 \cdot RH\ cott^2$   
 $- 0.0031583333 \cdot RH\ cott + 0.0570058594$   
 For  $RH \leq 15\%$  :  $WADS (\%rate/min) = 0.025$  (6a)

For  $RH > 15\%$  :  $WDES(\%rate/min)$   
 $= -\left(0.00000007383 \cdot RH\ cott^3 - 0.00000260307$   
 $\cdot RH\ cott^2 - 0.00018394526 \cdot RH\ cott$   
 $+ 0.01318569610\right)$  For  $RH$   
 $\leq 15\%$  :  $WDES (\%rate/min) = 0.01$  (6b)

To deal with factor 2 (cotton  $EMC$  at different  $RH\ cott$  values) the values for each  $EMC$  from the adsorption and desorption are close enough to use the average of both.

Similarly, we have adjusted a 4th order equation polynomial (7) using the same fitting method as above to data of  $EMC$  versus  $RH\ cott$  values from Xie et al. [21 Fig. 8a], which are shown in our Fig. 4a:

For  $RH \leq 95\%$  :  $EMC$   
 $= 0.0000002567 \cdot RH\ cott^4 - 0.0000079435$   
 $\cdot RH\ cott^3 - 0.0021949318 \cdot RH\ cott^2$   
 $+ 0.2075227420 \cdot RH\ cott$   
 For  $RH > 95\%$  :  $EMC = 14$   
 $+ (RH - 95)/1.25$  (7)

To use these Eqs. (6a, 6b and 7) we need the  $RH\ cott_{i-1}$  value calculated by Eq. (1b).

To solve the differential equation of  $RH\ cott = function (WADS, WDES, EMC, t)$  according the Eqs. (6a, 6b and 7) we use a numerical FEM method with the same time steps used at “Humidity change at the void from the vapour permeation through the canvas (Partial process 1)” and “Humidity change at the void from the air infiltration flow (Partial process 2)” sections and as explained in “Calculation procedure by time steps” section. The calculations in this case are more complex as the variable  $EMC$  implies a set of 4 conditionals for each of the three

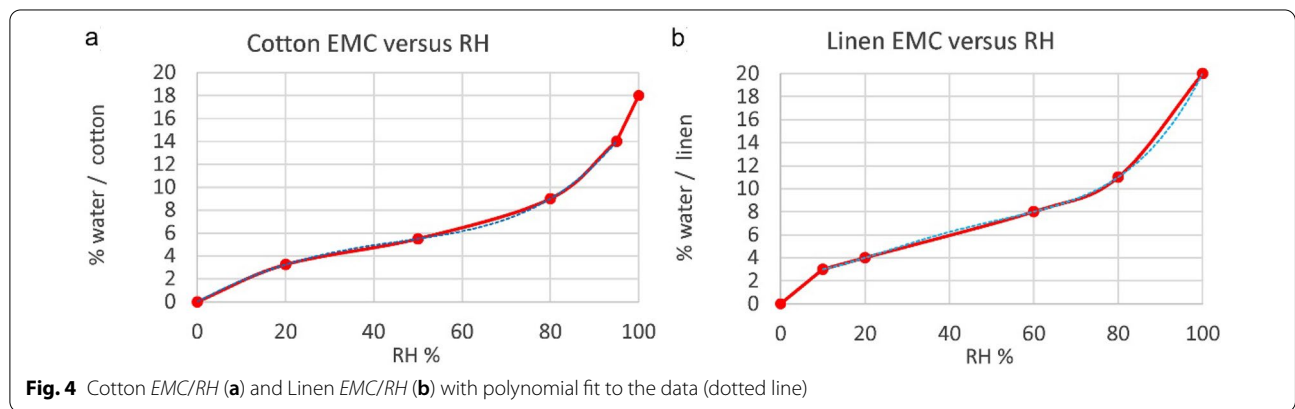


Fig. 4 Cotton  $EMC/RH$  (a) and Linen  $EMC/RH$  (b) with polynomial fit to the data (dotted line)

Table 1 Conditionals to select  $\Delta SCott\%$ ,  $MCCott\%$ , and  $\Delta SVoidCott\%$

Processes	Conditionals for cotton and canvas sorption	$\Delta SCott\%$ , and $\Delta SCanv\%$	$MCCott\%$ , and $MCCanv\%$ ,	$\Delta SVoidCott\%$ , and $\Delta SVoidCanv\%$ ,
Adsorption	$MC_{i-1} < EMC_i$ and $MC_{i-1} + WADS > EMC_i$	$EMC_i - MC_{i-1}$	$EMC_i$	$MC_{i-1} - EMC_i$
Adsorption	$MC_{i-1} < EMC_i$ and $(MC_{i-1} + WADS = EMC_i$ or $MC_{i-1} + WADS < EMC_i)$	$WADS$	$MC_{i-1} + WADS$	$- WADS$
Desorption	$MC_{i-1} > EMC_i$ and $(MC_{i-1} + WDES > EMC_i$ or $MC_{i-1} = EMC_i)$	$WDES$	$MC_{i-1} + WDES$	$- WDES$
Desorption	$MC_{i-1} > EMC_i$ and $MC_{i-1} + WDES < EMC_i$	$EMC_i - MC_{i-1}$	$EMC_i$	$MC_{i-1} - EMC_i$

For the Canvas change  $Cott$  by  $Canv$

secondary variables: the moisture content of the cotton layer ( $MCCott_i$ ), its change ( $\Delta SCott_i$ ), and the change of moisture of the void ( $\Delta SVCott_i$ ), listed in Table 1. These conditionals ensure, firstly, that  $MC\% < EMC\%$  in each time step. Secondly, that if  $MC\% > EMC\%$  the remaining vapour goes to the air void, as it is not adsorbed by the cotton. The equations used to implement these conditionals within the Excel model tool can be seen in Additional file 1. Note that, in order to obtain the sorption and desorption rates with the correct units, the rate in (% rate/min) needs to be multiplied by  $\Delta ts \cdot 60$ .

From the  $\Delta SVoidCott_i$  value, we find the vapour mass variation at void from cotton sorption in step “i” ( $\Delta SVoidCott_i$ ) as:

$$\Delta SVoidCott_i = (\Delta SVoidCott_i/100) \cdot Mcott \quad (8)$$

After we calculate the  $Mvapcott_{i-1}$  (void vapour mass from cotton sorption before the “i” step):

$$Mvapcott_{i-1} = (Vol \cdot \rho aircott_i) \cdot MRvoid_{i-1} \text{ being} \quad (9a)$$

$$\rho aircott_i = 1,2 \cdot \left( \frac{293}{273 + Tcott_i} \right) \text{ and after it :} \quad (9b)$$

$$MRvoidsorp_cott_i = (Mvapcott_{i-1} + \Delta SVcott_i) / (Vol \cdot \rho aircott_i) \quad (9c)$$

$$\Delta MRvoidsorp_cott_i = MRvoidsorp_cott_i - MRvoid_{i-1} \quad (9d)$$

#### Humidity change at the void from the vapour sorption in the linen canvas (Partial process 4)

The linen canvas vapour sorption is the fourth partial process involved. Based on the same process described for cotton vapour sorption, we have adjusted the equations for linen vapour sorption rate (%/min) versus RH linen and for EMC versus RH linen. The polynomial equations are adjusted from the values at Xie et al. [21 Figs. 4c and 8c].

The equations for linen adsorption WADS (%rate/min) and desorption WDES (%rate/min) are:

$$\begin{aligned} \text{For } RH > 60\% : WADS(\%rate/min) &= -0.0000000008 \cdot RH canv^4 + 0.0000001725 \\ &\cdot RH canv^3 - 0.0000080980 \cdot RH canv^2 \\ &+ 0.0000280392 \cdot RH canv + 0.0093647059 \\ \text{For } RH \leq 60\% : WADS(\%rate/min) &= 0.009 \end{aligned} \quad (10a)$$

$$\begin{aligned} \text{For } RH > 10\% : WDES(\%rate/min) &= - \left( 0.00000005728 \cdot RH canv^3 - 0.00000423503 \right. \\ &\cdot RH canv^2 + 0.00008068687 \\ &\cdot RH canv + 0.00862248789) \\ \text{For } RH \leq 10\% : WDES(\%rate/min) &= 0.009 \end{aligned} \quad (10b)$$

For linen, the EMC versus RH canv graphic is shown in our Fig. 4b and the equation obtained is:

$$\begin{aligned} \text{For } RH > 10\% : EMC &= 0.00000007937 \cdot RH canv^4 - 0.0001230159 \\ &\cdot RH canv^3 + 0.0062301587 \cdot RH canv^2 \\ &- 0.126984127 \cdot RH canv + 2.6190476190 \\ \text{For } RH \leq 10\% : EMC &= 0.3RH canv \end{aligned} \quad (11)$$

To use these Eqs. (10a, 10b and 11) we need the  $RH canv_{i-1}$  calculated by Eq. (1b). As above, the differential equation for  $RH canv = function(WADS, WDES, EMC, t)$  according the Eqs. (10a, 10b and 11) is solved with a numerical FEM method. In this process the variable EMC, also implies a set of 4 conditionals for each of the three secondary variables ( $SorpCanv_i\%$ ,  $MCCanv_i\%$  and  $\Delta SVCanv_i\%$ ). These variables are calculated with the same conditionals expressed in Table 1.

From the  $\Delta SVoidCanv_i$  value, we find the vapour mass variation at void from canvas sorption in step “i” ( $\Delta SVoidCanv_i$ ) as:

$$\Delta SVoidCanv_i = (\Delta SVoidCanv_i/100) \cdot Mcanv \quad (12)$$

Following this, we calculate the  $Mvapcanv_{i-1}$ , which is the void vapour mass from canvas sorption before the “i” step, as well as the increase in this time step:

$$Mvapcanv_{i-1} = (Vol \cdot \rho aircanv_i) \cdot MRvoid_{i-1} \quad (13a)$$

$$\rho aircanv_i = 1,2 \cdot (293/(273 + Tcanv_i)) \quad (13b)$$

$$MRvoidsorp_canv_i = (Mvapcanv_{i-1} + \Delta SVCanv_i) / (Vol \cdot \rho airvoidcanv_i) \quad (13c)$$

$$\Delta MRvoidsorp_canv_i = MRvoidsorp_canv_i - MRvoid_{i-1} \quad (13d)$$

The general concepts explained in points 3.5 and 3.6, related to the sorption process (adsorption and desorption) and EMC in cellulose fibers are applicable to others fibers with different hygroscopic properties, which will



require updated equations for adsorption–desorption. Similar data can be found in Xie et al. [21, Figs. 4 and 8] who calculated the sorption rate and EMC values for other fibres such as as hemp or jute.

**Total MR at void and RH at the different layers at the end of each time step**

The differential equations modelling the mixing ratio MR changes along the temperature cycles have been solved numerically for each of the partial processes equations in parallel as shown from “Humidity change at the void from the vapour permeation through the canvas (Partial process 1)” to “Humidity change at the void from the vapour sorption in the linen canvas (Partial process 4)” sections. The total MR change at the void is the sum of the changes caused by all the partial processes, which leads to the following expression for Cases 1 and 3 as:

$$MR\ void_i = MR\ void_{i-1} + \Delta MR\ void\ perm_i + \Delta MR\ inf_i + \Delta MR\ void\ sorp\ canv_i \tag{14a}$$

This equation is slightly modified for Case 2 and 4, by replacing the increase in moisture through sorption in the canvas ( $\Delta MR\ void\ sorp\ canv$ ) by the same increase in the cotton layer ( $\Delta MR\ void\ sorp\ cott$ ). The rationale for

this change is described in “Cycle temperatures calculation for each time step” section.

$$MR\ void_i = MR\ void_{i-1} + \Delta MR\ void\ perm_i + \Delta MR\ inf_i + \Delta MR\ void\ sorp\ cott_i \tag{14b}$$

Knowing the MR allows the calculation of the Relative Humidity at the air boundary layer adjacent to the cotton layer, the canvas and aluminium ( $RH\ cott_i$ ,  $RH\ canv_i$  and  $RH\ alum_i$ ) at the end of the “i” time step and at the start of time step “i + 1”. From  $MR\ void_i$  we calculate the RH of each layer ( $RH\ layer_i$ ) with Eq. (1b) for the canvas, cotton, or aluminium as layers, with the added conditionals:

$$RH\ layer_i = 100\% \text{ if the calculated } RH\ layer_i > 100\% \text{ to limit RH if condensation happens.} \tag{15a}$$

$$RH\ layer_i < 0\% \text{ if the calculated } RH\ layer_i = 0\% \text{ used only as indicator if calculations goes wrong.} \tag{15b}$$

This completes the calculations within the current time step “i”, for which we have obtained  $MR\ void_i$ ,  $RH\ cott_i$ ,  $RH\ canv_i$  and  $RH\ alum_i$ . With the value of  $MR\ void$  in time step “i”, and the values of  $T\ room$ ,  $T\ canv$ ,  $T\ cott$ ,  $T\ alum$  and  $MR\ room$  in the next time step “i + 1”, we can

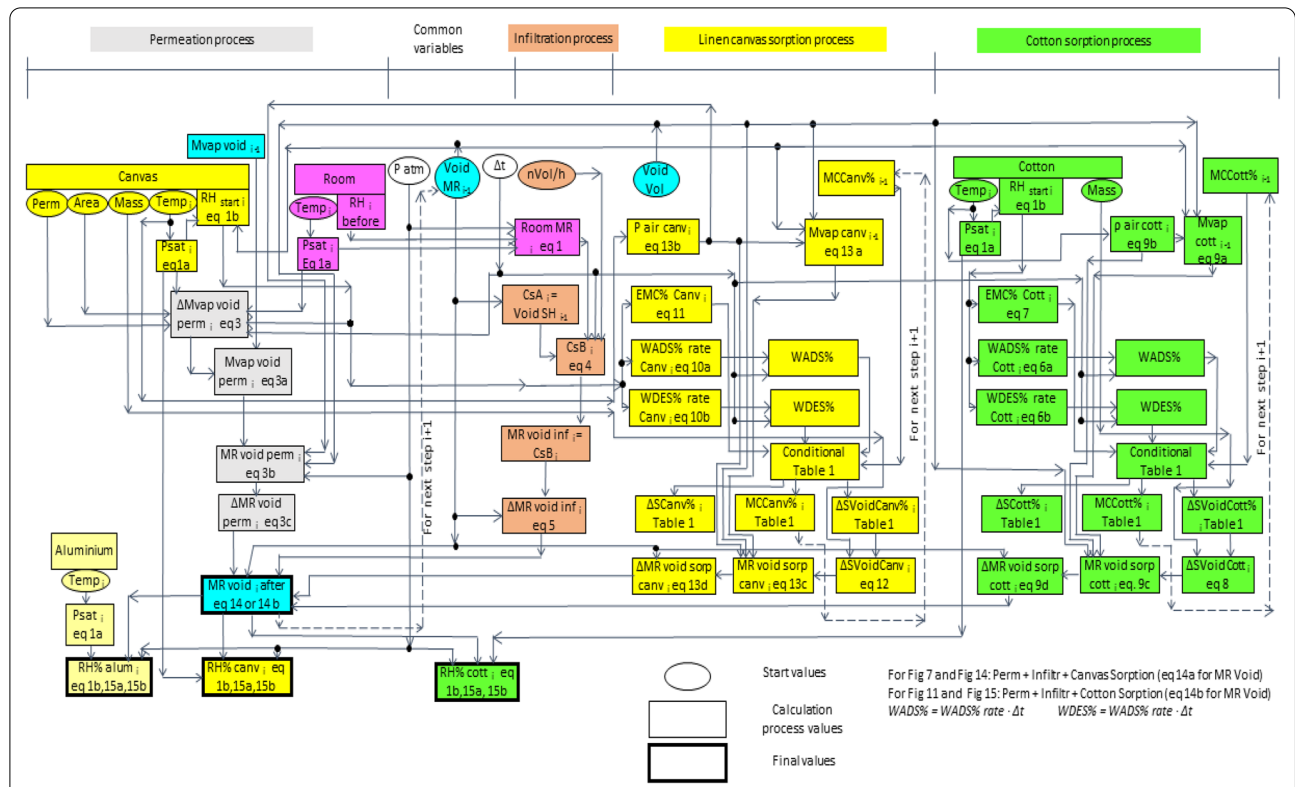


**Fig. 5** Diagram for the complete model process calculations in each time step “i”. The boxes indicate variables. The arrows indicate how variables are used to calculate other variables

calculate first the new  $RH$  values at room, canvas, cotton and aluminium with Eq. (1b) and after all the variable values of the time step “ $i + 1$ ” with the same equations as in time step “ $i$ ”. We can repeat the same calculation process over one or more cycles.

In order to clarify the complete model process calculations, we include in Fig. 5 a diagram with the calculation variables and the reference of the equations involved in time step “ $i$ ”.

#### Software used for the simulation model

The simulation can be done with software like Visual Basic, Excel macros, Python, or others. We have used Excel files, one for each case, carrying out each time step calculations for *Vapour Canvas permeation + Air infiltration + Cotton sorption + Canvas sorption* and the final step *MR void* in one line. We have chosen Excel because it is ubiquitous, user-friendly, and accessible. In order to obtain the required accuracy and a stable calculation along the time it is necessary to adjust the value of the time-step,  $\Delta t$ , which is different in each studied Case.

- Case 1, 2 (2 cycles of 4 h each):  $\Delta t = 0.00033$  h,  $\Delta t s = 1.2$  s (48,000 Excel lines).
- Case 3 with 2 cycles of 24 h each:  $\Delta t = 0.001$  h,  $\Delta t s = 3.6$  s (48,000 Excel lines).
- Case 4 (2 cycles of 24 h each) at  $\Delta t = 0.00025$  h,  $\Delta t s = 0.9$  (192,000 Excel lines).

This number of rows is supported by the Excel tool. Longer experiments could potentially reach the limit of rows, and thus require alternative software.

#### Model parameters

To check our simulation model, we have used in all the cases the same dimensions and materials as in Padfield [16], a commercial canvas (0.6 m  $\times$  0.5 m) with a factory applied ground and a white acrylic paint layer, weighting 134 g and 0.447 kg/m<sup>2</sup>. As this commercial canvas has one open woven layer of linen and other layer of ground, we have assumed in our calculations a density of 0.335 kg/m<sup>2</sup> for the linen canvas which corresponds to a 75% of the total. Thus, we estimate that the mass of canvas available for sorption and permeation is 100.5 g, while the mass of the ground layer is 33.5 g.

For vapour permeance flow, the white acrylic paint layer is the main barrier to the vapour flux compared with the other layers as the canvas and the factory applied ground (see Table 2). According to it, the vapour permeance used is 9.90E–11 kg/(m<sup>2</sup> s Pa) from the acrylic primed canvas at [12] and correspond to the material used at [16]. The void depth between the canvas and the aluminium back plate is 29 mm and the real void

volume (excluding the stretcher and the cross-beam) is 0.00669 m<sup>3</sup>.

Our model can deal with permeance values from 1.00–E13 to 1.00E–09 kg/(m<sup>2</sup> s Pa) which are normal in the treated canvas used by painters. Around 1.00E–08 may appear instabilities in the calculations.

In our simulation models corresponding to [16 Figs.7, 11, 14 and 15] we use a 0.4 Vol/h air infiltration rate that corresponds to a value obtained at [16] by flushing nitrogen into the void and measuring the oxygen return by an optical method.

The woven cotton layer (0.632 kg/m<sup>2</sup> and 189 g) used in our models is located inside the void and stuck to the aluminium back plate in Case 2, and at 3 mm gap of the canvas in Case 4, as in [16 figs. 11 and 15] corresponding to ours Figs. 7d and 9d.

#### Model simulation results and discussion

The model predictions agree with the experimental data, as demonstrated in Fig. 6. The amplitude and shape of the predicted fluctuations coincide with the experimental data, but display a slight delay. Despite this difference, the model predicts accurately the range of values of  $RH$  and  $MR$  within the canvas. Figures 7, 8, 9 and 10 compare the experiments by Padfield et al. with [Figs. 7, 11, 14 and 15 of reference 16] with the output of the simulations. The alignment between experiments and simulations is so close, that including them into all the figures would result in excessive overlap of the lines. For visual clarity, we have chosen to display an example of a comparison between experiments and simulations in Fig. 6.

The remaining figures in this section contain simulation and experiments side to side, to provide a clearer visualisation. The reader can find in Appendix A, Table 5 a detailed comparison between these simulated cases and the experimental graphics for the same cases from [16].

The original experimental data [Figs. 7, 11, 14 and 15 of reference 16] display a small difference between the canvas surface  $RH$  and the near canvas  $RH$ . Differences also appear between the surface canvas and near canvas temperature, the aluminium surface  $RH$  and the  $RH$  near the aluminium  $RH$ , and the surface aluminium temperature

**Table 2** Materials, permeances and references

Materials	kg/(m <sup>2</sup> s Pa)	References
Acrylic primed canvas	9.90E–11	Di Pietro [12]
Canvas + size + ground + oil paint	6.6E–10	Hendrickx [22]
canvas size + ground	4.2E–09	Hendrickx [22]
Canvas not treated	1.00E–08	Hendrickx [22]
Canvas linseed oil	2.74E–10	Di Pietro [12]

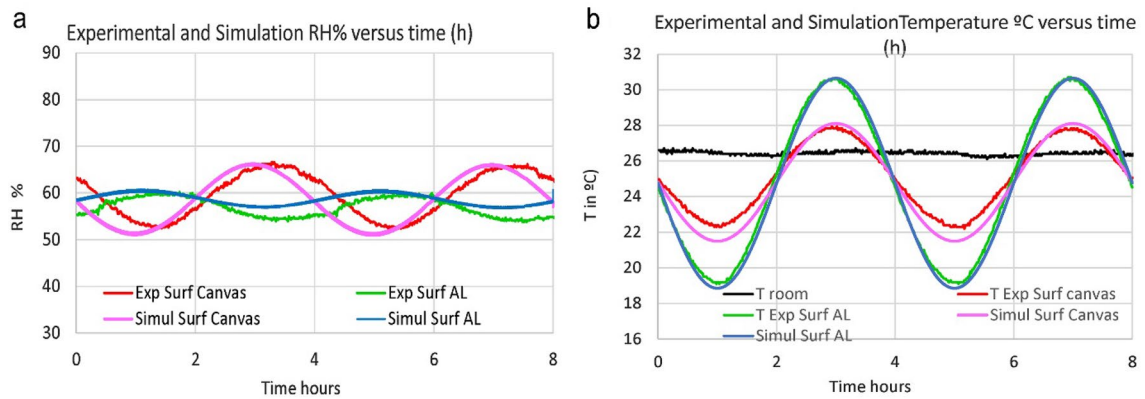


**Fig. 6** Comparison of simulated and experimental *RH* values with the same temperature cycles and start values of *MR* Void and Room for Case 2. *RH* (a) and temperature (b)

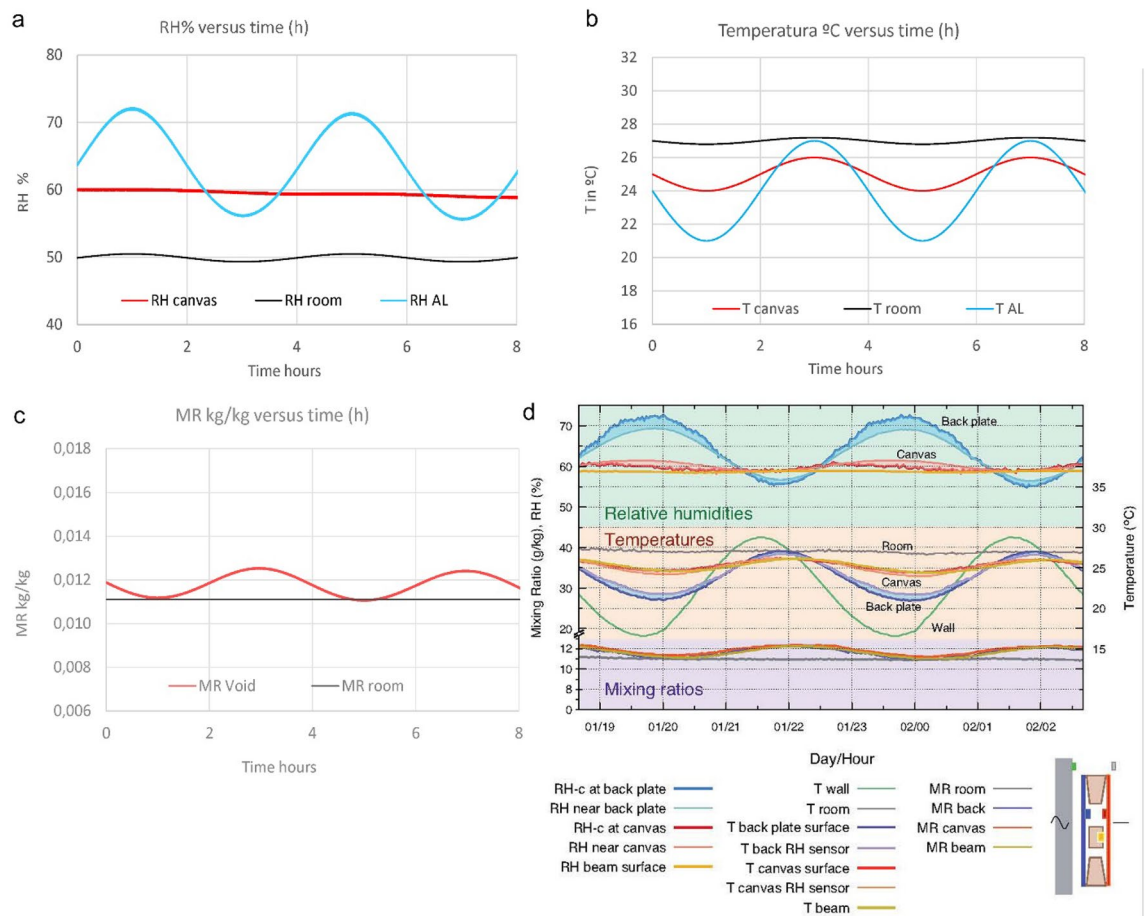


**Fig. 7** Case 1. Model M (1–3) simulation with conditions of Case 1. *RH* (a), temperature (b), *MR* (c) and the complete graphic from Padfield et al. [16] Fig. 7], to compare with them (d)

and the temperature near the aluminium. The reason for these discrepancies is that the *RH* Honeywell sensors used in [16] measure the *RH* near the surface but not at the surfaces and the temperature thermocouple and PT-100 sensors measure the surface temperature values. The *RH* values at the surfaces at [16] are calculated from the *MR Void* and the surface temperatures and thus are more accurate than the near surface *RH* and temperature values. In our simulation model we have calculated the *RH* and temperature values at the surfaces (not near the surfaces) and thus they shall be compared with the surface *RH* and temperature values.

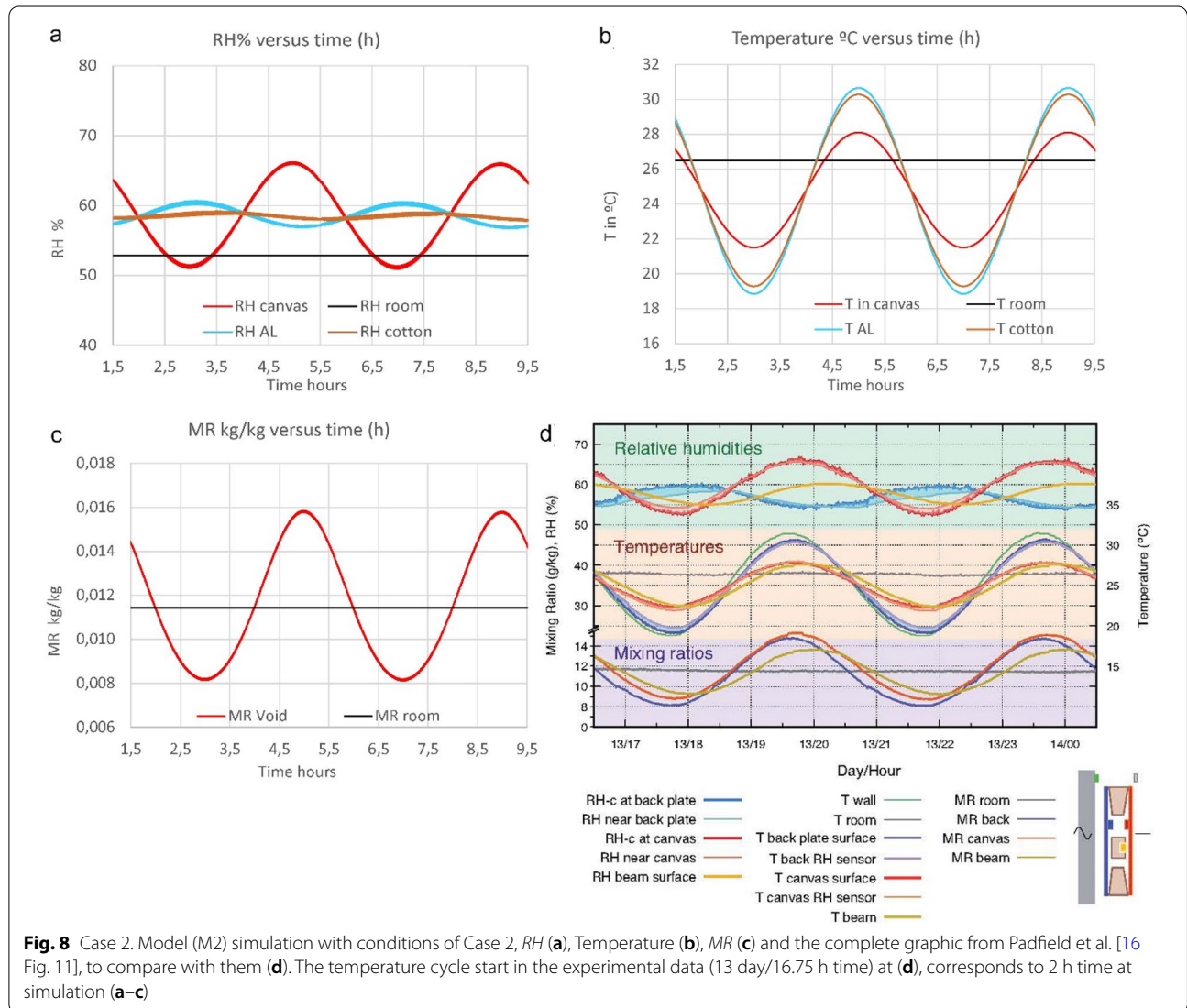
**Results for Case 1**

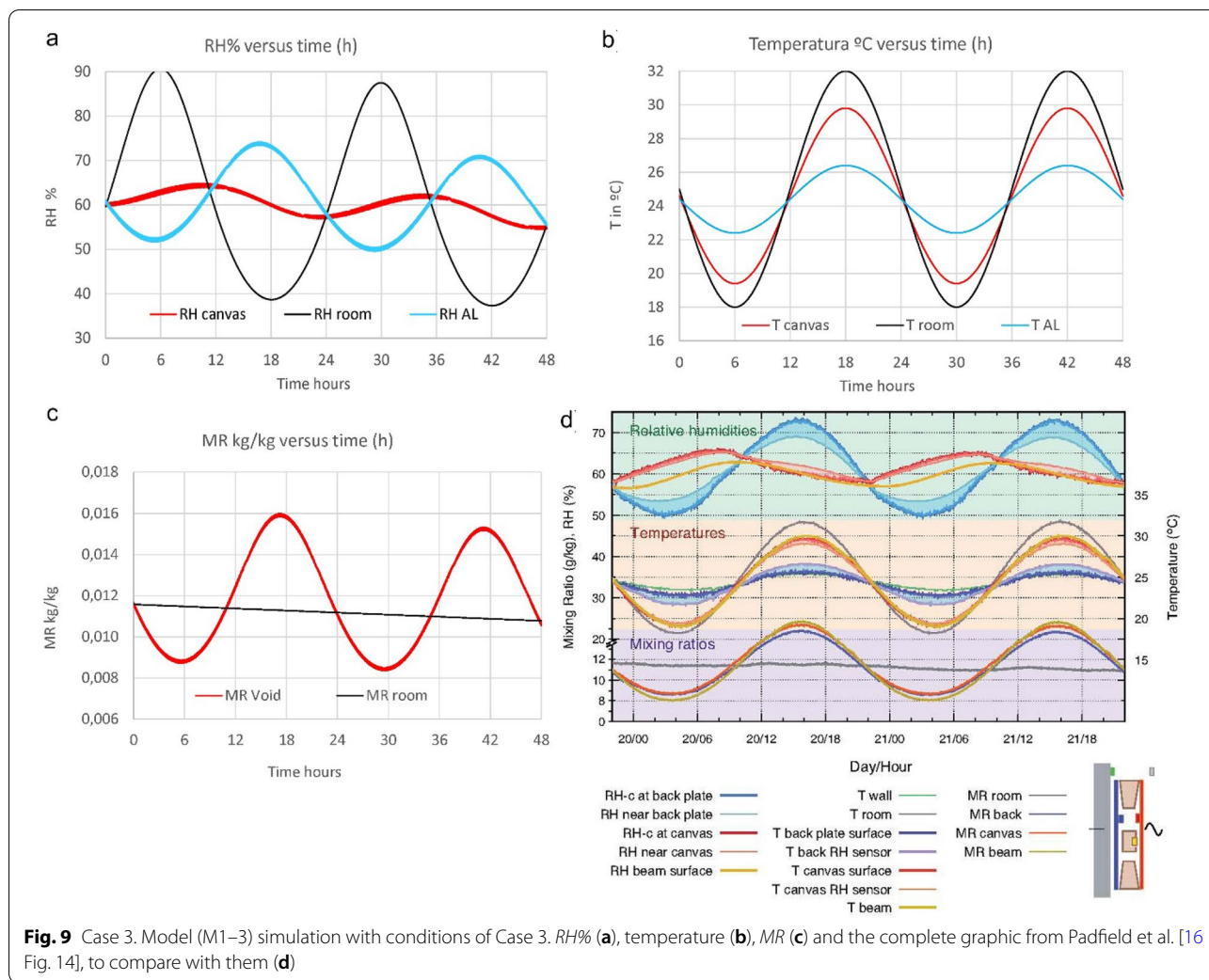
Our results for this case are shown at Fig. 7a–c and agree with the experimental values along the cycles shown at

Fig. 7d which is the same as [16 Fig. 7]. The canvas has a nearly constant *RH* (60% to 59%) but at the aluminium back plate *RH* oscillates between 72 and 56%. With more extreme conditions the water condensation will occur before in the aluminium back plate than in the canvas due his greater temperature oscillation. With this simulation model researchers can predict the *RH* values attained inside the canvas/aluminium void according to the room and the wall conditions, testing different scenarios not covered by the original experiments.

**Results for Case 2**

In case 2, the best fit to the experimental data (half cycle delay in the canvas *RH* values to the ones expected from the canvas temperatures) is obtained by assuming that the canvas is at the equilibrium moisture content along





the cycles. If adsorption and desorption fluxes to the canvas were included in the simulation, the results would show a small discrepancy in magnitude and cycle delay. This indicates that the moisture content of the canvas responds very quickly to external changes, and that the assumption of a resistance to a moisture flux adds an unrealistic delay in the mass exchange. To account for this, we have considered that the canvas is in constant equilibrium with its surroundings, and that the moisture exchange through it affects the moisture in the void without altering the equilibrium of the canvas. In other words, in Case 2 the canvas does not participate in the vapour adsorption/desorption process, and consequently the canvas sorption shall not be taken in account in the calculations. Therefore we have not included the term  $\Delta MR_{void\ sorp\ canvas}$  in Eq. 14b.

Proceeding in this manner the results of our simulation of Case 2 agree with the experimental values along the cycles shown at Fig. 8d which is the same as [Fig. 11

from Ref. 16]. See Fig. 8a–c. In our graphics we also show the calculated cotton *RH* values from cotton temperatures very close to the ones of the aluminium as both are in close contact.

In the aluminium air boundary layer, at minimum temperature the *RH* attains its maximum value as shown in the Fig. 8a and [16 Fig. 11] and thus the *RH* values in the aluminium air boundary layer are not delayed to those expected according to their cycle temperatures.

### Results for Case 3

Our results for this case are shown at Fig. 9a–c and agree with the experimental values along the cycles shown at Fig. 9d which is the same as [16 Fig. 14]. In Fig. 9a we show the calculated room *RH* which was not represented in the [16 Fig. 14] but it can be deduced from the temperatures and *MR* values.

Two interesting facts are visible in our simulation and in the experimental values: (1st) the aluminium back

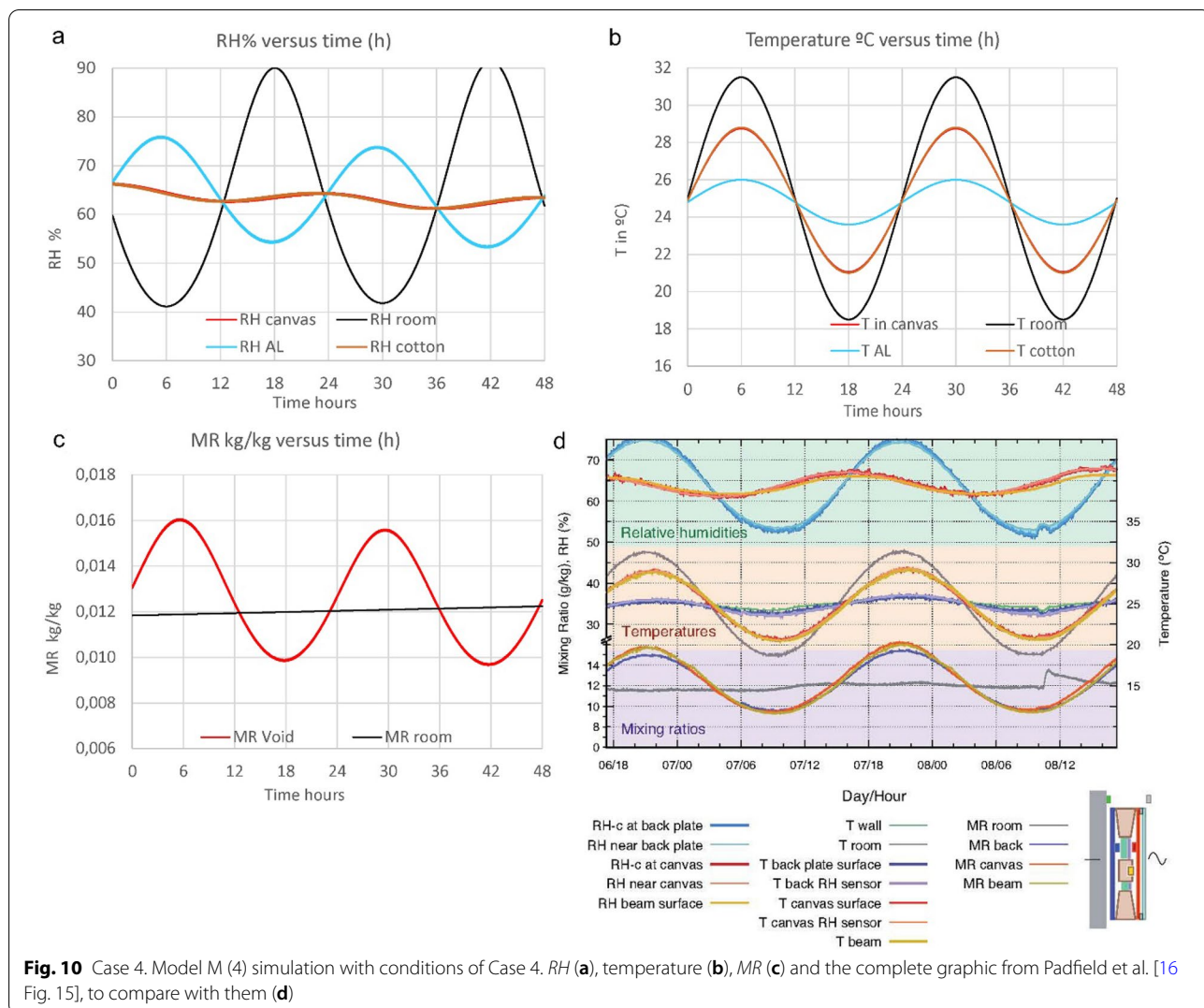


plate *RH* values show a half cycle delay to the expected values from their temperatures. (2nd) the canvas *RH* values are delayed near a quarter of a cycle to the expected values from their temperatures.

According to our simulation model, both facts can be explained as follows: the canvas linen has a high hygroscopic capacity to adsorb and desorb water but this process is limited by two factors, one is the sorption rate and the other one is the *EMC*, both varying according to the air void *RH* near the canvas linen. Our simulation model explains, through the conditionals summarised in Table 2, how the interaction between the linen sorption rate and the *EMC* produces these delays. These conditionals limit the water transference between the air and the hygroscopic materials, causing the vapour to accumulate temporarily in the void, delaying the canvas and cotton cycle *RH* values to those expected according to the temperatures cycles.

It is interesting to note that the average mixing ratio in the void approaches gradually, over time, the mixing ratio of the room. This is visible in the maximum value of the fluctuations of moisture in the void seen in Fig. 9c, where the second fluctuation has a markedly smaller average value.

**Results for Case 4**

Our results for this case are shown at Fig. 10a–c and agree with the experimental values along the cycles shown at Fig. 10d which is the same as [16 Fig. 15]. In our graphics we also show the calculated cotton and room temperatures and *RH* values.

This case displays the same unexpected phenomena seen in Case 3: the aluminium back plate *RH* values show a half cycle delay to the expected values from their temperatures and the canvas *RH* values are delayed nearly a quarter of a cycle in relation to the expected values from

their temperatures. Once again, the conditions summarised in Table 2 ensure that the model accounts successfully for this phenomena. As above, the average void  $MR$  approaches gradually the room  $MR$ , as seen in Fig. 10c.

#### Complementary cases: changes in the textile layers

We have simulated some complementary cases to improve the understanding of the involved phenomena. In reality, only a minority of canvases are purely made of cotton. In many cases natural and synthetic materials are mixed, which results in a reduction of the buffering capacity of the textile layers. To explore this scenario, we have added the following cases:

Case 2.1: As Case 2 with model M (2) but cotton mass only 20% of its cotton mass.

Case 3.1: As Case 3 with model M (1–3) but canvas mass only 20% of its canvas mass.

Case 4.1: As Case 4 with model M (4) but cotton mass only 20% of its cotton mass.

The common trend observed in these new cases is that the reduction of mass of hygroscopic material causes increased fluctuations in the canvas in comparison with the original cases. In addition, all cases show different delays in the fluctuations of  $RH$  in the various layers (Fig. 11).

Finally, we have simulated other cases where we have changed the vapour permeance of the canvas or the infiltration rate. The results of these simulations are shown in Table 3. For each simulated case, we have recorded two outputs: (1) the  $RH$  cycle delays in relation to an “ideal” scenario, where the maximum  $RH$  coincides with the minimum  $T$ . (2) the range of  $RH$  at the different layers. The nomenclature used in Table should be interpreted as follows: Case 1 is the original case, Case 1.A includes a change in the permeance, and Case 1.B includes a change in the infiltration rate.

The results of Table 4 demonstrate the difficulty of making simple generalisations: a change in permeance or ventilation can have different effects depending on the configuration of the protective layer. For example, an increase in ventilation rate, as a general rule, does not increase the range of fluctuations of  $RH$  in the canvas. However, in Case 3, which does not have a layer of cotton, an increase of permeation or ventilation results in an increase of internal fluctuations, from 61/59 in Case 3 to 74/46 in Case 3.A.3 and 70/49 in 3.B. This is because, in this case, the canvas is the only hygroscopic layer that can mitigate fluctuations.

The model also allows users to evaluate the risk of condensation under any combination of  $T$  and  $RH$ . In Table 4, we provide a few examples of model results,

obtained by changing the values of average  $T$ , fluctuation amplitude and  $RH$  of Case 2. These results show that condensation can occur with relatively low values of humidity in the room and canvas, in particular when there are significant temperature differences between the front and the back of the painting. Large differences of humidity between the room and the canvas also result in increased risk of condensation. The values provided in Table 4 are by no means applicable to all scenarios: on the contrary, they are very specific to the conditions of Case 2. Nonetheless, they illustrate the ability of the model to assess risks in a range of environmental scenarios.

#### Conclusions

At present and historically, reverse protections have been applied in order to minimize the degradation that can occur in canvas paintings due to humidity fluctuations. However, the moisture buffering provided by the protective layers is difficult to predict. What happens inside these layers is a complex series of water transfer processes, all of them interrelated.

The unknown consequences of adding a protection, and the possible adverse consequences for the paintings that a new microenvironment may create, are a cause of concern to conservators who are aware of these risks and who may be hesitant to apply back protection when climatic conditions are uncontrolled or adverse.

Tim Padfield and his team carried out a very interesting experimental work in their last paper *Back protection of canvas paintings* [16], which presents experimental data of what happens in a protected painting that is subjected to different climatic conditions.

In this paper we have developed a complete physical–mathematical model to simulate the evolution of  $RH$  and  $MR$  at the different easel painting layers when the room and the wall were submitted to temperature cycles, which results in temperature cycles in each layer. The layers of interest are the canvas, the ground, the white acrylic paint film, the aluminium back plate protection and, in some cases, a glass on the front and/or a cotton layer inside the void. To evaluate the model, we have compared the results of our simulations with the experimental values obtained in Figs. 7, 11, 14 and 15 of [16] in the same conditions.

The model successfully reproduces the experimental results by Padfield et al. Our approach is based on the assumption that the experimental observations can be reproduced by taking into account four interrelated processes: canvas permeation, air infiltration in the void, cotton sorption and linen sorption.

Our model can explain some surprising features of the experimental data. Namely, it is able to capture several instances where temperature and relative humidity

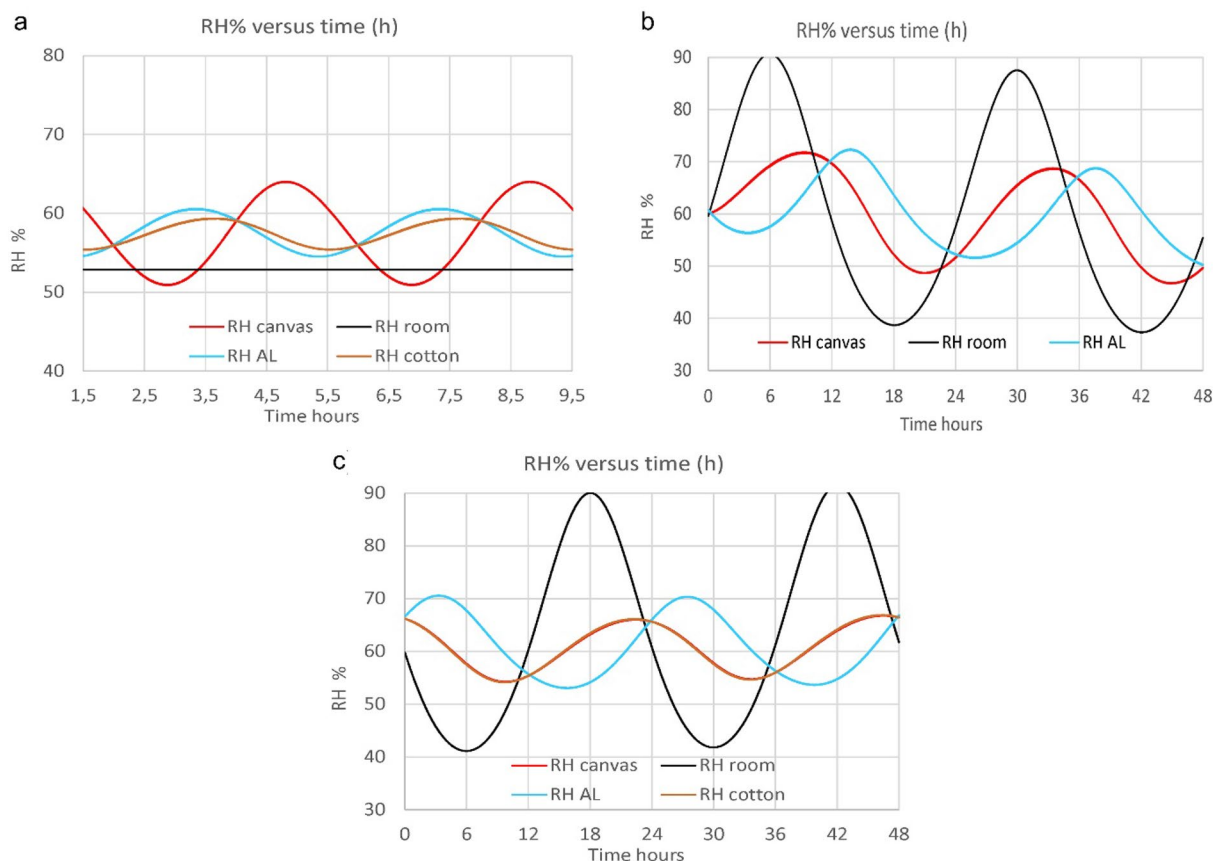


**Fig. 11** RH simulation results for complementary cases: Case 2.1 (a), Case 3.1 (b) and Case 4.1 (c)

rise simultaneously, which runs contrary to the common situation in which minimums of  $T$  correspond to maximums of  $RH$ . This occurs in the following instances: the rise of  $RH$  near the canvas when the temperature rises in the Case 2 (Fig. 8a and b) and the rise in  $RH$  near the aluminium when its temperature rises in the Case 3 (see Fig. 9a and b). The model also successfully captures the delay between the  $RH$  values and those expected at their temperatures. These trends appear to be caused by the limited vapour adsorption capacity of cotton and linen materials at different  $RH$ , which we reproduce by modelling the Equilibrium Moisture Content and the vapour sorption rate values at different  $RH$  in accordance with their adsorption/desorption mode.

After validating the model against experimental data, we extend it to additional cases. This allows the exploration of a diversity of scenarios: changing the permeance of the canvas and the infiltration rate of air, as well as testing different materials with smaller percentages of cotton, and thus reduced buffering capacity. The model is also able to predict the risk of condensation under

temperature and humidity gradients between the front and the back of the painting. In summary, the proposed model contains two useful innovations for preventive conservation. Firstly, it provides a physical framework that helps interpret complex experimental observations. Secondly, it provides a practical tool, which can be run in common spreadsheet software, for predicting the consequences of back protection in any environment. The model contains two important assumptions: (1) that the wooden stretcher has a negligible buffering capacity in comparison to the other hygroscopic materials in the system, (2) that the transport of moisture is not limited by gradients of moisture within the layers. While valid in the studied case, the applicability of these two simplifications needs to be assessed carefully when the model is used in other scenarios. In particular, future research should determine in which cases the wooden stretcher might contribute significantly to buffering. In addition, if future research clarifies the interaction between moisture and wood, it would be useful to introduce this process in the model in order to quantify its relative importance.



**Table 3** Summary of results of cases where permeance and infiltration are changed

Case	Permeance (vapour) kg m <sup>-2</sup> s <sup>-1</sup> Pa <sup>-1</sup>	Infiltration rate nVol/h	RH cycle delays to the ideal values at the void layers temperatures			RH interval (max/min) % in 1st cycle		
			Canvas	Cotton	Aluminium	Canvas	Cotton	Aluminium
1	1.00E-12	0.4	0		0	60/59		72/56
1.A	1.00E-09	0.4	1/2		0	60/53		71/50
1.B	1.00E-12	10	1/4		0	60/58		72/55
2	1.00E-12	0.4	1/2	1/4	0	65/52	59/58	60/56
2.A.1	1.00E-11	0.4	7/16	1/4	1/8	65/52	58/60	57/61
2.A.2	1.00E-10	0.4	7/16	1/4	1/8	65/52	58/58.5	56.5/60.5
2.A.3	1.00E-09	0.4	7/16	1/4	1/8	64/50	60/54	61/53
2.B	1.00E-12	10	7/16	1/4	1/16	64/50.5	59/55.5	60/54.5
3	1.00E-12	0.4	3/16		7/16	61/59		72/50
3.A.1	1.00E-11	0.4	3/16		5/16	62/59		73/50
3.A.2	1.00E-10	0.4	3/16		5/16	65/68		74/52
3.A.3	1.00E-09	0.4	2/16		17/32	74/46		72/52
3.B	1.00E-12	10	3/16		5/16	70/49		72/50
4	1.00E-12	0.4	1/4	1/4	1/2	66/61.5	66/61.5	75/54
4.A	1.00E-09	0.4	1/8	1/8	3/8	67/52	67/52	70/53
4.B	1.00E-12	10	3/16	3/16	7/16	65/57	65/57	72/52

The outputs are cycle delays in relation to an ideal case (maximum RH and minimum T coincide) and RH range at different layers. Cases indicated a N, N.A and N.B, where N denotes the original Cases 1-4, A denotes change in permeance, and B denotes change in infiltration rate

**Table 4** Condensation for various extreme conditions of T and RH at room, canvas, cotton and aluminium in Case 2

RH start %	Location	Temp. average °C	ΔT± K	RH max %	Temp. average °C	ΔT± K	RH max %	Temp. average °C	ΔT± K	RH max %	Temp. average °C	ΔT± K	RH max %
52	Room	20	1	56	15	1	56	28	1	56	22	1	56
58.2	Canvas	19	2	66	14	2	65	26	2	66	20	2	65
	Cotton	13	3.5	88	13	3.5	63	19	3.5	92	15	3.5	82
	Alum	12	4	97	12	4	70	18	4	100	14	4	90
60	Room	20	1	64	15	1	64	28	1	65	22	1	64
50	Canvas	19	2	57	14	2	56	26	2	57	20	2	56
	Cotton	13	3.5	75	13	3.5	55	19	3.5	79	15	3.5	71
	Alum	12	4	83	12	4	61	18	4	87	14	4	78
70	Room	20	1	75	15	1	75	28	1	75	22	1	75
30	Canvas	19	2	36	14	2	35	26	2	36	20	2	36
	Cotton	13	3.5	48	13	3.5	34	19	3.5	52	15	3.5	46
	Alum	12	4	53	12	4	38	18	4	57	14	4	50
30	Room	20	1	32	15	1	32	28	1	33	22	1	32
70	Canvas	19	2	76	14	2	78	26	2	73	20	2	79
	Cotton	13	3.5	100	13	3.5	76	19	3.5	100	15	3.5	99
	Alum	12	4	100	12	4	84	18	4	100	14	4	100
70	Room	20	1	75	15	1	75	28	1	75	10	1	75
60	Canvas	19	2	68	14	2	67	26	2	69	8	2	64
	Cotton	13	3.5	91	13	3.5	65	19	3.5	95	3	2.5	88
	Alum	12	4	100	12	4	72	18	4	100	1	3	100
30	Room	20	1	32	15	1	32	10	1	32	5	1	32
30	Canvas	19	2	34	14	2	34	8	2	32	4	2	32
	Cotton	13	3.5	45	13	3.5	33	2	2.5	47	0	2.5	34
	Alum	12	4	50	12	4	36	0	3	58	-2	3	52

ΔT indicates the amplitude of the T fluctuations

**Table 5** Variables correspondence between our paper and Padfield et al. [16 Figs. 7, 11, 14 and 15]

Variables	Simulation results data shown in our paper	Experimental data from Ref [16] shown in our paper	Experimental data shown in Ref [16]
Room and void start $T, RH, MR$ from Ref [16]	Figures 7a–c, 8a–c, 9a–c, 10a–c	Figures 7d, 8d, 9d, 10d	Figures 7, 11, 14, 15
Cycle $\Delta T$ in all layers from Ref [16]	Figures 7b, 8b, 9b, 10b		
Case 1 all layers $RH, MR$	Figure 7a and c	Figure 7d	Figure 7
Case 2 all layers $RH, MR$	Figure 8a and c	Figure 8d	Figure 11
Case 3 all layers $RH, MR$	Figure 9a and c	Figure 9d	Figure 14
Case 4 all layers $RH, MR$	Figure 10a and c	Figure 10d	Figure 15

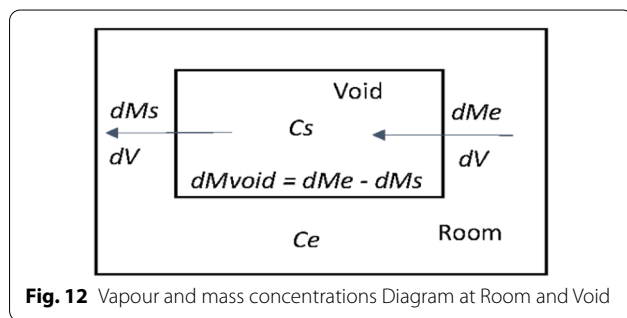


**Fig. 12** Vapour and mass concentrations Diagram at Room and Void

Future research will focus in the creation of an interactive application that makes this model accessible to any user, regardless of their technical ability.

**Appendix A. Variables correspondence between our paper and Ref. [16]**

For an easy understanding about the correspondence between the Padfield et al. [16] experimental data and our simulation results we include Table 5 showing the variables correspondence between our paper graphics and her graphics.

**A.1 Air infiltration flow inside the canvas/aluminium void**

Following Padfield [16] suggestion about considering the water vapour flow from the room to the void, due to the air infiltration through the space between the canvas and the stretcher, we have introduced in our model the infiltration air flow. The process to model how the  $MR void_i$  change by the air infiltration flow along the “i” time step, uses the variables:  $\rho rate_i, Ce_i, Cs_i, Me_p, Ms_p, Mvoid_p, dV_p, V_{AB}, Vol void, nVol/h$ , (see Fig.

12) with  $\Delta t = t_i - t_{i-1}$  as time step and the following relations between them:

Vapour concentration at the void:  $Cs = MR void$

Vapour concentration at the room:  $Ce = MR$

$$\begin{aligned}
 & \text{Air volume infiltrated at void in } dt: && \text{room } dV \\
 & \text{Vapour mass coming into the void} && dMe = \rho_{air room} \cdot dV \cdot Ce \\
 & \text{Vapour mass exiting from the void} && dMs = \rho_{air void} \cdot dV \cdot Cs \\
 & \text{Vapour mass variation inside the void} && dMvoid = Vol void \cdot \rho_{air void} \cdot dCs \\
 & \text{Air density rate} && \rho rate = \rho_{air room} / \rho_{air void}
 \end{aligned}$$

From these relations we get:

$$\begin{aligned}
 dMvoid &= dMe - dMs = \rho_{air room} \cdot dV \cdot Ce \\
 &\quad - \rho_{air void} \cdot dV \cdot Cs = \rho rate \cdot \rho_{air void} \cdot dV \cdot (Ce - Cs) \\
 (Ce - Cs) &= Vol void \cdot \rho_{air void} \cdot dCs
 \end{aligned}
 \tag{16}$$

The required volume to reach  $Cs$  is:

$$dV = \frac{Vol void \cdot dCs}{\rho rate \cdot (Ce - Cs)}
 \tag{17}$$

Integrating between conditions A and B with  $CsA$ , (vapour concentration in the void at conditions A, time step start) and  $CsB$  (the same magnitude at conditions B, time step end):

$$\begin{aligned}
 VAB &= \int_{VA}^{VB} dV = \frac{Vol void}{\rho rate} \int_{CsA}^{CsB} \frac{dCs}{Ce - Cs} \\
 &= - \frac{Vol void}{\rho rate} \int_{CsA}^{CsB} \frac{dCs}{Cs - Ce}
 \end{aligned}
 \tag{18}$$

$$VAB = - \frac{Vol void}{\rho rate} \cdot (\ln(Cs - Ce))_{CsA}^{CsB} + K$$

$$VAB = - \frac{Vol void}{\rho rate} \cdot (\ln(CsB - Ce) - \ln(CsA - Ce)) + K$$

$$V_{AB} = -\frac{Vol\ void}{\rho\ rate} \cdot \ln \frac{C_{sB} - C_e}{C_{sA} - C_e} + K \tag{19}$$

In condition A we have  $Vol_{AB} = 0$  and  $C_{sB} = C_{sA}$

$$0 = -Vol \cdot \ln(1) + KK = (Vol\ void / \rho\ rate) \cdot \ln(1) = 0$$

$$V_{AB} = -\frac{Vol\ void}{\rho\ rate} \cdot \ln \frac{C_{sB} - C_e}{C_{sA} - C_e} \tag{20}$$

$$\frac{-V_{AB}}{Vol} \cdot \rho\ rate = \ln \frac{C_{sB} - C_e}{C_{sA} - C_e}$$

$$\exp\left(\frac{-V_{AB}}{Vol} \cdot \rho\ rate\right) = \frac{C_{sB} - C_e}{C_{sA} - C_e} \tag{21}$$

$$C_{sB} = C_e + (C_{sA} - C_e) \cdot \exp\left(\frac{-V_{AB}}{Vol} \cdot \rho\ rate\right) \tag{22}$$

As the rate  $Vol_{AB}/Vol\ void$  is the required number of void volumes to get  $C_{sB}$ , with time  $\Delta t$  we get:

$$\frac{nVol}{h} \cdot \Delta t = \frac{V_{AB}}{Vol}$$

and thus

$$C_{sB} = C_e + (C_{sA} - C_e) \cdot \exp(-\Delta t \cdot nVol/h \cdot \rho\ rate) \tag{23}$$

By the air infiltration process at the end of time step “i”:  $MR\ void\ inf_i = MR_B = C_{sB}$

$$\Delta MR\ void\ inf_i = MR\ void\ inf_i - MR\ void_{i-1} \tag{24}$$

**Abbreviations**

t: Time (h);  $\Delta t$ : Time step value (h);  $\Delta t_s$ : Time step value (s); *i* (subindex): Time step number;  $\omega$ : Total cycle time (h);  $\beta$ : Initial cycle phase (radians); *Factor T*: Temperature oscillation harmonic factor; *void*: Space between canvas and aluminium; *room*: Room air; *canv*: Canvas air boundary layer in the void; *cott*: Cotton air boundary layer in the void; *alum*: Aluminium air boundary layer in the void; *T*: Temperature °C; *RH*: Air relative humidity ( $0 < RH < 100$ ); *MR*: Mixing ratio kg water/kg dry air; *MR void*: Mixing ratio in the void; *MR void perm*: MR void from permeation; *MR void inf*: MR void from infiltration; *MR void sorp cott*: MR void from cotton sorption; *MR void sorp canv*: MR void from canvas sorption; *MR room*: MR in the room;  $\Delta MR\ void$ : MR variation by time step in the void;  $\Delta MR\ void\ perm$ :  $\Delta MR$  void from permeation;  $\Delta MR\ void\ inf$ :  $\Delta MR$  void from infiltration;  $\Delta MR\ void\ sorp\ cott$ :  $\Delta MR$  void from cotton sorption;  $\Delta MR\ void\ sorp\ canv$ :  $\Delta MR$  void from canvas sorption; *patm*: Atmospheric pressure (Pa); *psat*: Saturation vapour pressure (Pa); *pvap*: Vapour pressure (Pa); *pvap canv*: Vapour pressure in void near the canvas (Pa); *pvap room*: Vapour pressure in the room (Pa); *pvap cott*: Vapour pressure in void near the cotton (Pa); *pvap alum*: Vapour pressure in void near the aluminium (Pa); *P*: Vapour permeance (kg/(m<sup>2</sup> s Pa)); *A*: Canvas area (m<sup>2</sup>); *M*: Total mass of hygroscopic material (kg);  $\rho$ : Density (kg/m<sup>3</sup>);  $\rho\ air\ canv$ : Dry air density near canvas (kg/m<sup>3</sup>);  $\rho\ air\ cott$ : Dry air density near cotton (kg/m<sup>3</sup>);  $\rho\ rate$ :  $\rho\ air\ room/\rho\ air\ void$ ; *Vol*: Void air volume (m<sup>3</sup>); *Mvoid*: Vapour mass in the void (kg); *Me*: Vapour mass coming inside the void (kg); *Ms*: Vapour mass going outside the void (kg); *Ce*: Room vapour concentration (kg vapour/kg dry air); *Cs*: Void vapour concentration (kg vapour/kg dry air); *CsA*: Void *Cs* at initial state A (kg vapour/dry air); *CsB*: Void *Cs* at state B in time t (kg vapour/kg dry air); *dV*: Air going in or out the void in time t (m<sup>3</sup>); *V<sub>AB</sub>*: Air infiltrated from state A to state B (m<sup>3</sup>); *Vol/h*: Air infiltration rate in the void; *nVol*: Number of

void air volumes infiltrated; *nVol/h*: Number of void air volumes by hour; *EMC*: Equilibrium moisture content (max %mass water/mass cotton or linen) at an *RH* value; *MC<sub>cott</sub>%*: Moisture content (% mass water/mass cotton); *MC<sub>canv</sub>%*: Moisture content (% mass water/mass canvas); *WADS*: Water adsorption rate %; *WDES*: Water desorption rate %;  $\Delta Sorp\ Cott\%$ : Cotton sorbed water %;  $\Delta SVoid\ Cott\%$ : Water vapour variation at void from cotton sorption (% of cotton mass);  $\Delta SVoid\ Cott$ : Water vapour mass variation at void from cotton sorption (kg);  $\Delta Sorp\ Canv\%$ : Canvas sorbed water (%);  $\Delta SVoid\ Canv\%$ : Water vapour variation at void from canvas sorption (% of canvas mass);  $\Delta SVoid\ Canv$ : Water vapour mass variation at void from canvas sorption (kg); *Mvap canv*: Void vapour mass for canvas sorption (kg); *Mvap cott*: Void vapour mass for cotton sorption (kg); *Mcott*: Cotton mass (kg); *Mcanv*: Canvas mass (kg).

**Supplementary Information**

The online version contains supplementary material available at <https://doi.org/10.1186/s40494-022-00741-2>.

**Additional file 1.** Case 1 evolution of Temperature (a), RH (b), EMC (c) and MR (d) in the Void at the Canvas boundary layer between 2 h and 2,06 h of the cycle time.

**Acknowledgements**

We dedicate this paper to the memory and legacy of Tim Padfield’s excellent conservation research.

**Author contributions**

The order of authors in this paper has been set applying the sequence-determines-credit approach (SDC). SF developed the mathematical model, carried out the calculation procedure and was a major contributor in writing the manuscript. GC-F contributed to the global approach as a conservator, provided conservation literature background and contributed to the discussion of results. IB-M contributed to the discussion from the conservation point of view, the writing process and prepared the manuscript for final publication. AN-T participated in the discussion of the results from the conservation point of view. All authors read and approved the final manuscript.

**Funding**

This research did not receive any specific grant from funding agencies in the public, commercial, or not-for-profit sectors.

**Availability of data and materials**

The datasets used and/or analyzed during the current study are available from the corresponding author on reasonable request.

**Declarations**

**Competing interests**

The authors declare that they have no competing interests.

**Author details**

<sup>1</sup>Independent Researcher, Domènec Oristrell, 55. esc. C, 2<sup>a</sup>-3<sup>a</sup>, 08173 Sant Cugat del Vallès, Spain. <sup>2</sup>Arts and Conservation Department, Fine Arts Faculty, University of Barcelona, C/Pau Gargallo 4, 08028 Barcelona, Spain. <sup>3</sup>Institute for Sustainable Heritage, University College London, London, UK.

Received: 4 January 2022 Accepted: 19 June 2022

Published online: 22 July 2022

**References**

1. Mecklenburg MF. Microclimate and moisture induced damage to paint layers. In: Padfield T, Borchersen K, editors. Museum microclimates conference. Copenhagen: The National Museum of Denmark; 2007. p. 19–25.
2. Mecklenburg MF, Tumosa CS. Mechanical behavior of paintings subjected to changes in temperature and relative humidity. In: Mecklenburg,

- Marion F, editors. *Art in transit: studies in the transport of paintings*. Washington, DC: National Gallery of Art; 1991. p. 173–216.
3. Von Reden A. Uncertainties in the interactions between a canvas painting support and moisture. In: Ashley-Smith J, Burmester A, Eibl M, editors. *Climate for collections. Standards and uncertainties. Postprints of the Munich climate conference 7–9 Nov 2012*. Doerner Institut; 2013. p. 247–256.
  4. Berger GA, Russell WH. Deterioration of surfaces exposed to environmental changes. *J Am Inst Conserv*. 1990;29(1):45–76. <https://doi.org/10.2307/3179590>.
  5. Russell WH, Berger GA. The behaviour of canvas as a structural support for painting: preliminary report. *Stud Conserv*. 1982;27(1):139–45. <https://doi.org/10.1179/sic.1982.27.Supplement-1.139>.
  6. Michalski S. Paintings: their response to temperature, relative humidity, shock, and vibration. In: Mecklenburg, Marion F, editors. *Art in transit*. Washington, DC: National Gallery; 1991. p. 223–48.
  7. Michalski S. The ideal climate, risk management, the ASHRAE chapter, proofed fluctuations, and towards a full risk analysis model. In: Boersma F, editor. *Contribution to the experts roundtable on sustainable climate management strategies, held in April 2017 in Tenerife, Spain*. Los Angeles: The Getty Conservation Institute; 2007.
  8. Museums, galleries, archives and libraries. In: Owen MS, editor. *ASHRAE handbook—HVAC applications*. Atlanta: ASHRAE-American Society of Heating, Refrigerating and Air Conditioning Engineers Inc.; 2011:23. p. 23-1–23-2.
  9. UNE-EN 15757 Conservation of cultural property—Specifications for temperatures and relative humidity to limitate the climate-induced mechanical damage in organic hygroscopic materials. Brussels: European Committee for Standardisation; 2010.
  10. Ferrer S, Campo-Francés G, Ruiz-Recasens C, et al. Microclimate numerical simulation to obtain the minimum safe distances between a painted wood panel and the inner face of an exterior wall. *Herit Sci*. 2020;8:34. <https://doi.org/10.1186/s40494-020-00376-1>.
  11. Grau-Bové J, Mazzei L, Strlic M, et al. Fluid simulations in heritage science. *Herit Sci*. 2019;7:16. <https://doi.org/10.1186/s40494-019-0259-9>.
  12. Di Pietro G, Ligterink FJ. Prediction of the relative humidity response of backboard-protected canvas paintings. *Stud Conserv*. 1999;44(4):269–77. <https://doi.org/10.1179/sic.1999.44.4.269>.
  13. Ligterink FJ, Di Pietro G. Canvas on cold walls: relative humidity differences near the stretcher (Section 5). In: Padfield T, editor. *Museum microclimates: contributions to the Copenhagen conference, 19–23 November 2007*. Copenhagen: National Museum of Denmark; 2007:5, p. 27–38.
  14. Dixon T. Framing, glazing, backing, and hanging of paintings on canvas. *Conserv Easel Paintings*. 2012;44:727–32.
  15. Nicolai K. *Manual de restauración de cuadros (Handbuch der Gemälderestaurierung)*; 1998. p. 115.
  16. Padfield T, Padfield N, Lee DSH, et al. Back protection of canvas paintings. *Herit Sci*. 2020;8:96. <https://doi.org/10.1186/s40494-020-00435-7>.
  17. Thybring EE, et al. Kinetics of water vapor sorption in wood cell walls; state of the art and research needs. *Forests*. 2019;10:704.
  18. Henry PSH. The diffusion of moisture and heat through textiles. *Discuss Faraday Soc*. 1948;3:243–57. <https://doi.org/10.1039/DF9480300243>.
  19. Código Técnico de la Edificación (CTE). Documento Básico HE Ahorro de energía. Appendix G.3.1. Ecuaciones G.14 y G.15. International Thomson Editores, Spain Paraninfo, S.A.; 2008. p 92.
  20. Ceylan O, Goubet F, De Clerck K. Dynamic moisture sorption behaviour of cotton fibres with natural brown pigments. *Cellulose*. 2014;21:1149–61. <https://doi.org/10.1007/s10570-014-0206-6>.
  21. Xie Y, Hill CAS, et al. The dynamic water vapour sorption behaviour of natural fibres and kinetic analysis using parallel exponential kinetics model. *J Mater Sci*. 2011;46:479–89. <https://doi.org/10.1007/s10853-010-4935-0>.
  22. Hendrickx R, Desmarais G, Weder M, et al. Moisture uptake and permeability of canvas paintings and their components. *J Cult Herit*. 2016;19:445–53. <https://doi.org/10.1016/j.culher.2015.12.008>.

### Publisher's Note

Springer Nature remains neutral with regard to jurisdictional claims in published maps and institutional affiliations.

Ready to submit your research? Choose BMC and benefit from:

- fast, convenient online submission
- thorough peer review by experienced researchers in your field
- rapid publication on acceptance
- support for research data, including large and complex data types
- gold Open Access which fosters wider collaboration and increased citations
- maximum visibility for your research: over 100M website views per year

At BMC, research is always in progress.

Learn more [biomedcentral.com/submissions](https://biomedcentral.com/submissions)

